EasyChair Preprint

№ 13229

The Establishment of a Hypoxia Cellular Morphology Model Based on Deep Convolutional Neural Networks and Intelligent Screening of Anti-Hypoxia Drugs

Xinyi Zhang and Zheng Wang

May 8, 2024

The Establishment of a Hypoxia Cellular Morphology Model Based on Deep Convolutional Neural Networks and Intelligent Screening of Anti-Hypoxia Drugs

Xinyi Zhang,School of Chemical Engineering and Technology, Tianjin University, Tianjin, China
Zheng Wang*,College of Intelligence and Computing,Tianjin University, Tianjin, China

***Abstract*—The rapid development of artificial intelligence has brought many innovative achievements to fields such as drug design and drug discovery [1]. Combining traditional graphics methods with deep learning methods can significantly improve the accuracy of drug screening.**

Hypoxia refers to the process in which tissues or cells in the body undergo abnormal changes in morphology, physiological functions, and metabolism due to insufficient oxygen supply or oxygen utilization obstacles [2]. Hypoxia is a major characteristic of high-altitude environments, so it is crucial to prevent and treat cardiovascular diseases related to hypoxia.

Enlargement of the cell nucleus is a recognizable morphological feature of hypoxic cells. Based on a deep learning multi-cell image classification model, this study constructed a high-throughput compound screening system for discriminating the anti-hypoxic activity of thousands of compounds. By simultaneously performing prediction scoring using AC16 and H9C2 models, the anti-hypoxic activity of thousands of compounds was predicted, and some compound molecules with anti-hypoxic effects were successfully screened. Therefore, morphology-based CNN systems can become powerful tools for screening antioxidant drugs.

***Index Terms*—Screening of anti-hypoxia drugs , Convolutional Neural Networks, Deep learning**

I. Introduction

Due to the rapid advancement of Convolutional Neural Networks (CNNs), the accuracy of image classification tasks has significantly improved. CNNs have been widely applied in the field of drug development and screening, and morphology-based identification systems using CNNs can, in some tasks, replace molecular biology techniques [3]. By employing artificial intelligence and machine learning methods, screening models can sift through vast amounts of compounds to identify potential drug candidates. Selecting suitable compounds and conducting activity experiments through screening models can greatly enhance the efficiency of drug development, reduce costs, and provide more possibilities for the discovery of new drugs techniques [4].

Oxygen is a crucial substance for energy metabolism, serving as the energy source for vital biological processes in mammals [5]. It is essential for physiological functions and metabolism in mammals. Hypoxia is a widely studied condition that profoundly affects cellular metabolism, migration, and vascular genesis during development and disease processes.

Hypoxia is one of the primary characteristics of high-altitude environments, and inadequate adaptation to low-oxygen environments can lead to altitude sickness. Prolonged myocardial hypoxia can disrupt the energy metabolism of myocardial cells, leading to myocardial cell damage and cardiac remodeling. Hypoxia-related cardiovascular diseases have a high mortality and morbidity rate worldwide, posing significant challenges for prevention and treatment.

Currently, both domestically and internationally, drugs used to treat altitude sickness mainly include traditional Western medicines such as acetazolamide [6], and acetazolamide inhibitors [7]. However, their preventive effects on altitude sickness are not ideal, and long-term use can cause significant adverse reactions. Therefore, there is a growing focus on seeking effective and low-toxicity candidate components from traditional Chinese medicine for the development of anti-hypoxia drugs for high-altitude regions.

However, due to the complex and diverse nature of Chinese herbal components, as well as the time-consuming and costly methods traditionally used to construct physical hypoxia models such as the liquid paraffin sealing method [8] [9], anaerobic bag gas production method, and the use of cobalt chloride [10], sodium hydrosulfite, and other chemicals to construct chemical hypoxia models for screening anti-hypoxia drugs, the development process is still in its early stages.

To address these issues, we have developed a hypoxia cell morphology recognition model based on deep convolutional neural networks, leveraging their strong image classification capabilities. This model can classify and identify cell images to assess and predict hypoxic cell morphology. Through extensive experiments, we have validated the accuracy and reliability of this model and established a hypoxia scoring system based on it, used to evaluate and screen novel anti-hypoxia small molecules. Additionally, we can conduct further mechanistic studies on the screened small molecules to explore their anti-hypoxia mechanisms and pharmacological activities, providing robust support and guidance for subsequent drug development efforts.

II. METHOD

A. Experimental Setting

1) Datasets: The dataset used in this paper was a home-made dataset. Two types of cardiomyocytes (rat cardiomyocytes H9C2 and human cardiomyocytes AC16) were used to be cultured in DMEM complete medium containing 10bovine serum and 1% penicillin-streptomycin double antibody, at 37°C and 5% CO2. Among them, AC16 cells were cultured in 12-well plates, and H9C2 cells were cultured in 35-mm dishes, which were dosed after 24H of culture and put into hypoxia chambers (95% N2, 5% CO2) for hypoxia treatment. After a period of hypoxia treatment, cells in each experimental and control set were imaged using an inverted microscope. 98-138 images were collected for each group for the training and validation sets, and 5 images were collected for each group for the test set with the addition of anti-hypoxia compounds

2) Implementation Details: All computer experiments were trained on an NVIDIA GeForce RTX 3090 with 24GB of video memory. The network parameters were randomly initialized; the initial learning rate was 0.0001; the batch size (batch size) was defaulted to 64; and the number of training rounds (epoch) was defaulted to 150. the learning rate was tuned using an exponential decay strategy, with the hyper-parameter gamma set to 0.98; and the learning rate was tuned and updated using the Adam optimizer.

B. Multi-cell Edge Extraction

In order to reduce the influence of image background on the cell classification task and improve the generalization performance of the model prediction, our method adopts an edge extraction method to process the edge of multi-cellular images as an image input to the prediction network. The edge extraction algorithm is implemented based on the Sobel operator, and its algorithmic flow is shown in Algorithm 1.

After the edge extraction algorithm, the input image is transformed from cell phase difference map to cell edge map, and the effect is shown in Figure 1. Edge extraction not only can initially extract the morphological features of cells, but also can suppress the background difference of the phase difference map, prevent the background difference of the phase difference map under the microscope caused by the different culture environment and acquisition time, and prevent the influence of the different background color on the model prediction. Since cell culture is time-consuming and costly, the amount of data obtained from the acquisition is small. In this paper, a series of data enhancement methods are used to expand the dataset. Data enhancement of the edge map was performed using random rotation 0-360°, vertical flip with probability 0.5 and horizontal flip with probability 0.5, and the enhanced image was scaled to 128×128 size and used as the input image for the expert network.

C. Morphological Feature Fusion Network

In the morphological feature fusion network proposed in this paper, the input cell edge image is firstly subjected to preliminary feature extraction and preliminary morphological

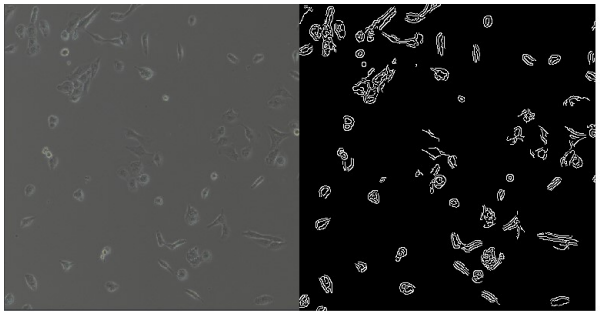

(a) edge extraction of AC16

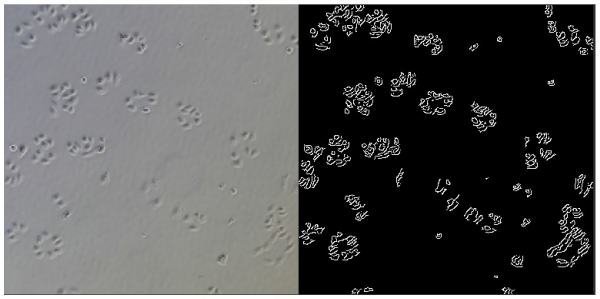

(b) edge extraction of H9C2

Fig. 1: Multi-cell edge extraction effect image

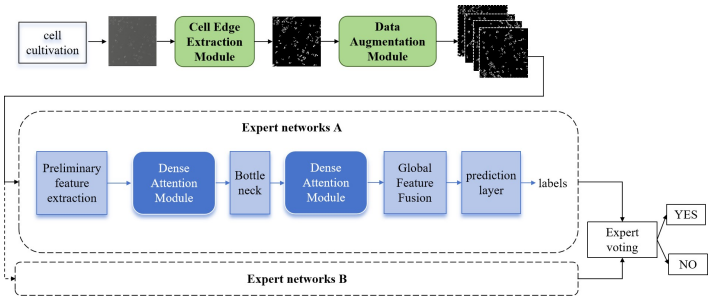

Fig. 2: Architecture of morphological feature fusion network

features F_1 are obtained; then advanced cell morphological features F_{att} are extracted by using the jump connection and attention module and the information between channels is learned and the number of channels is adjusted through the bottleneck layer; further morphological features are extracted by using the dense attention module and the loss of information in the process of feature extraction is compensated for, and the results F'_{att} are obtained; the edge features are fused with the advanced morphological features using average pooling, and then the prediction results for the hypoxia scoring of the image is outputted by using the fully connected layer and the softmax function. The network architecture is given in Figure2, and the specific process of orphological feature extraction and fusion is described in Algorithm2.

The results of a series of pre-experiments showed that the Dense Connectivity Module and the Attention Module each had different benefits for the two types of cells, AC16 and H9C2. In order to enhance the generalization of the expert

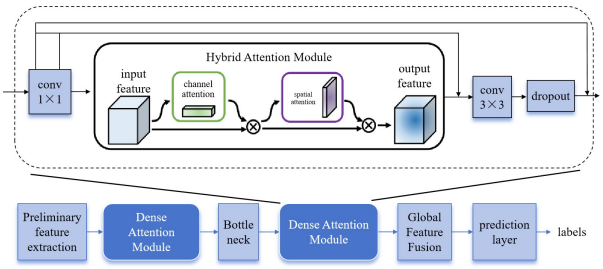

Fig. 3: Architecture of dense attention module

network to classify the two types of cells, a new dense attention module is designed in this paper.

1) Dense Attention Module: In dense attention module, the input features are firstly processed by 1×1 convolutional kernel to obtain F_1, which are added pixel-by-pixel with the initial input features as inputs to the attention module [11]; then the foreground feature enhancement and background feature suppression are performed on the summed features by using the serial channel attention mechanism and the spatial attention mechanism to obtain the attention features F_{space}; finally, pixel-by-pixel summation is performed again with the initial features and F_{space}, the final fusion of the summed features is performed by using 3×3 convolutional kernel to obtain the output features of the attention module. Finally, the initial input features are summed pixel by pixel again, and the summed features are finally fused using a 3×3 convolution kernel to obtain the output features of the dense attention module $F^{'}$. The details of dense attention module are illustrated in Figure3.

D. Multi-Expert Voting Intelligent Drug Screening

The multi-expert voting intelligent drug screening system has 10 input images, 5 phase difference maps each from AC16 cells and H9C2 cells collected after being cultured with the drugs to be tested, which are used to eliminate the experimental bias. Firstly, the edge extraction module was used to extract the edges of the 10 images; then the images were input into the corresponding morphological feature fusion expert networks for cellular morphological feature extraction and hypoxia morphology score prediction; finally, the respective hypoxia scores were averaged and compared with the control scores. The system retained compounds with hypoxia scores lower than those of the control group in the two expert networks as the effective anti-hypoxia drugs.

III. Result

In order to comprehensively and powerfully validate the effectiveness and advancement of the method in this paper, single cell morphology prediction method, simple feature extraction network prediction method, dense connectivity network prediction method and attention network prediction method were selected for performance comparison, and the screening results were validated by using the concentration gradient scheme of the known utility compounds and the correlation coefffcient scheme of the oxidative stress bioindicators. The accuracy, validity and sophistication of the method were veriffed in terms of machine learning metrics, biological metrics and cellular activity.

TABLE I: Experimental results of cellular hypoxia morphology recognition experiments

Datasets	Accuracy	Precision	Recall	F1
AC16-12H	0.806	0.817	0.823	0.806
AC16-24H	0.826	0.829	0.826	0.826
AC16-36H	0.970	0.962	0.976	0.968
AC16-48H	0.982	0.984	0.981	0.982
AC16-Hybrid	0.874	0.900	0.865	0.869
H9C2-24H	0.822	0.839	0.820	0.822
H9C2-36H	0.916	0.904	0.921	0.915
H9C2-48H	0.882	0.891	0.879	0.882
H9C2-Hybrid	0.874	0.879	0.875	0.874

A. Results of cellular hypoxia morphology recognition experiments

In this paper, AC16 and H9C2 were incubated with hypoxia for different durations, and the model was trained on the collected image data, and the results on the validation set are shown in TableI. The data in the table show that the model recognition becomes better as the incubation duration increases. This suggests that for AC16, 48H of anoxic hourly incubation can lead to an optimal anoxic morphological transition. And for H9C2, 36H is its optimal anoxic incubation duration. In order to improve the generalization of the model in the testing stage, we also used mixed dataset training for model training. As can be seen in the table, the model in this paper achieves F1 scores and accuracies of more than 0.8 for morphology classiffcation under multiple hypoxia duration culture conditions for both cells, and the highest even reaches 0.98.

B. Comparisons to the State-of-the-Art Methods

1) Simple feature extraction network prediction method: The Convolutional Neural Network (CNN) is a special type of feedforward neural network characterized by local connectivity and weight sharing [12]. As one of the core algorithms in deep learning, it is widely used in the field of computer vision. CNN serves as the foundational neural network architecture for many tasks such as image segmentation, object detection, and image classification models.

The convolutional layer is the most important component of a convolutional neural network (CNN). It performs convolution operations on the input data using convolutional kernels based on sliding windows, thereby extracting features from the input data [13]. The parameters in the convolutional kernels are updated through the backpropagation algorithm.

The Fully Connected Layers (FC) are an important structure within convolutional neural networks, acting as the "classifier" [14]. These layers aggregate the features extracted from the preceding layers and map the learned "distributed

feature representations" to the sample label space. Fully connected layers typically appear in the final few layers of a convolutional neural network, where they perform a weighted sum of the previously designed features.

Normalization operations stabilize the distribution of inputs in the intermediate layers of convolutional neural networks within an appropriate range, accelerating the model's convergence process and enhancing its stability to inputs of different sizes.

If a manually designed neural network relies solely on matrix operations in convolution, simple pooling, and normalization, it cannot effectively model and learn the complex feature space within 2D images. Activation functions introduce nonlinearity through simple function mappings, enhancing the model's learning and comprehension capabilities. The Softmax activation function is a commonly used neural network activation function, primarily used for multi-class classification problems. Its main purpose is to transform the output of a neural network into a probability distribution. Specifically, the Softmax function normalizes the output vector of the neural network, ensuring that their sum equals 1, thereby transforming the output vector into a probability distribution [15]. As a result, the sum of probabilities for each class equals 1, with each element of the output vector representing the probability of that class.

A simple convolutional neural network consists of three convolutional layers each using 3×3 kernels, followed by two fully connected layers. Batch normalization is applied after each convolutional layer, and the final fully connected layer outputs a tensor of dimension 2 [16]. The output from this layer passes through a Softmax activation function, enabling the outputs to represent the probabilities of the two categories: normal (0) and hypoxia (1).

As can be seen in TableII, the results indicate that the AC16 model performs worst at a cultivation duration of 24 hours, with prediction accuracy improving as the cultivation duration increases.However,it is unable to accurately model hypoxic morphology for AC16,and it is especially difffcult to achieve generalization under multiple time culture conditions. This is due to the fact that both cells, AC16 and H9C2, have gradual differences in morphology and individual differences with the passage of time under hypoxic environments, resulting in the fact that images obtained from culture environments captured at different time intervals may contain cells that fail to be completely hypoxic or have completed the hypoxic morphology transition ahead of time, as shown in Figure 4. In addition, the morphology presented during mitosis of AC16 cells is extremely similar to the hypoxic morphology, which also causes interference in CNN model classiffcation. This uncertainty in the dataset creates great difffculties for model training. From the experimental results of the single-cell morphology prediction method, it can also be seen that the prediction effect of the single-cell pictorial CNN model under 24h culture condition is signiffcantly lower than that under 48h culture condition.

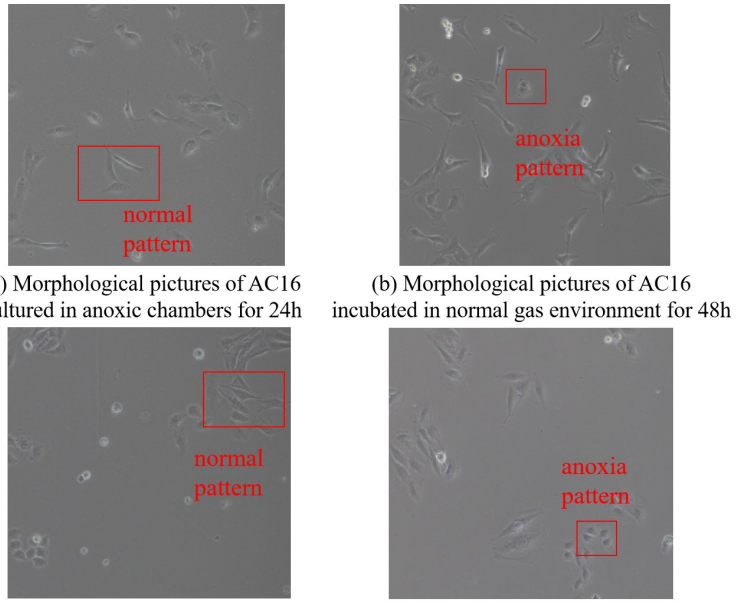

(a) Morphological pictures of AC16 cultured in anoxic chambers for 24h

(b) Morphological pictures of AC16 incubated in normal gas environment for 48h

(c) Morphological pictures of H9C2 cultured in anoxic chambers for 24h

(d) Morphological pictures of H9C2 incubated in normal gas environment for 48h

Fig. 4: Examples of cell culture images

2) Dense connectivity network prediction method: Dense connections pass low-level features to high-level convolutional blocks multiple times through skip connections, thereby supplementing high-resolution information in the higher convolutional layers. In a dense connection block, the input features are first dimensionally reduced along the channels using a 1×1 convolutional kernel. Then, further feature extraction is performed on the dimensionally reduced features using a 3×3 convolutional kernel. To prevent overfitting in CNNs, dropout regularization is applied at the end of the dense connection block [17].A bottleneck layer composed of 1×1 convolutional kernels and average pooling is added in multiple dense connection blocks to both reduce the number of channels and fuse features from different channels, thereby preventing excessive information aggregation in certain channels while also compressing the model.

From the experimental results(Table III):, it can be observed that dense connections significantly improve both the AC16 dataset at a single cultivation time and the mixed AC16 dataset at different cultivation times. However, there are still deficiencies in the recall metric.

3) Attention network prediction method: In convolutional neural networks, convolutional kernels extract local information from images through convolutional operations, weighting information equally across each region of the image using a sliding window. However, when humans observe images, they tend to focus on specific areas, a natural ability of the human brain known as visual attention mechanism. The attention mechanism fundamentally adjusts the weight distribution of the network towards important regions of interest, enhancing the model's ability to extract and represent features of the focused objects while suppressing irrelevant features

TABLE II: Experimental results in comparison with existing methods

method	datasets	F1	Accuracy	Precision	Recall
Single-cell morphology prediction method	AC16-24h	0.703597	0.735056	0.694856	0.712561
	AC16-48h	0.913023	0.930451	0.868515	0.922339
Our method	AC16-24h	**0.854384**	**0.848651**	**0.817972**	**0.894188**
	AC16-48h	**0.976621**	**0.977165**	**0.997297**	**0.956785**

TABLE III: Experimental results of ablation study

methods	datasets	F1	Accuracy	Precision	Recall
baseline	AC16-24h	0.794687	0.828631	0.787931	0.704123
	AC16-48h	0.912641	0.932145	0.867227	0.921725
	AC16-72h	0.932426	0.929246	0.804503	0.961900
	AC16-Hybrid	0.852473	0.864220	0.817241	0.940080
denseNet	AC16-24h	0.762424	0.785822	**0.857952**	0.686038
	AC16-48h	0.958079	0.958639	0.968226	0.948142
	AC16-72h	0.946227	0.948262	**0.997759**	0.899757
	AC16-Hybrid	0.944032	0.945556	0.962726	0.926050
AttentionNet	AC16-24h	0.800564	0.787750	0.750992	0.857143
	AC16-48h	0.972609	0.972766	0.978626	**0.976664**
	AC16-72h	0.924864	0.915000	0.927854	0.911891
	AC16-Hybrid	0.955899	**0.976250**	0.977138	**0.974662**
Our method	AC16-24h	**0.854384**	**0.848651**	0.817972	**0.894188**
	AC16-48h	**0.976621**	**0.977165**	**0.997297**	0.956785
	AC16-72h	**0.978606**	**0.979156**	0.995902	**0.961900**
	AC16-Hybrid	**0.962770**	0.964250	**0.997841**	0.940080

and reducing interference from unrelated objects. Attention aims to combine the advantages of attention mechanisms in both channel and spatial domains to compensate for the shortcomings in handling feature information across different dimensions.

The feature dimension obtained after convolutional layers is usually large, making it challenging for computers to process under limited computational resources. Pooling layers can reduce the feature dimension while retaining the effective information recorded in the feature matrix through pooling operations. The commonly used pooling operations include max pooling and average pooling [18].

The hybrid attention mechanism combines average pooling and max pooling to respectively obtain comprehensive and salient features from channel and spatial dimensions. These features are then fused using a multi-layer perceptron for channel dimension pooling features and via 1×1 convolution for spatial dimension pooling features. By incorporating the hybrid attention mechanism, CNNs can focus more on the parts of images that are most beneficial for image classification and suppress interference from irrelevant information when extracting multi-cellular features and establishing cellular image models.

From the experimental results(Table III), it can be seen that the hybrid attention mechanism significantly improves both the AC16 dataset at a single cultivation time and the mixed AC16 dataset at different cultivation times. However, there are still deficiencies in accuracy under the 24-hour cultivation condition.

4) Dense Attention Network prediction method: Through the two pre-experiments mentioned above, we found that dense connections and attention mechanisms each have different improvements on both the single-time cultivation and mixed datasets. In order to integrate the advantages of both and achieve a complementary effect, we propose a new cellular image CNN model.

In the Dense Attention CNN, we introduce a hybrid attention mechanism that considers both the position and content of input elements simultaneously, enabling more effective capture of essential information within the input. However, to further enhance the predictive performance of the CNN, we refine the hybrid attention mechanism by incorporating dropout and skip connections, forming the Dense Attention Module. Dropout randomly suppresses certain neurons during training to prevent overfitting, thereby improving the model's generalization ability. This allows the model to better focus on important features within the input during training while avoiding excessive fitting to non-essential features. Skip connections, on the other hand, are a special type of connection that directly passes the output of the hybrid attention processing to subsequent convolutional layers. This effectively compensates for any potentially lost vital information after hybrid attention processing, preventing information loss and enabling the model to consider various features within the

input more comprehensively.

With the aforementioned improvements, the predictive performance of the Dense Attention CNN on the AC16 dataset has been significantly enhanced(Table III). It can be observed that the Dense Attention Module, augmented with dropout and skip connections, notably improves the model's accuracy and generalization capability.

C. Ablation Study

In this paper, a series of ablation experiments are conducted on the dense attention module, and the results of the experiments are shown in TableIII. From the table, it can be seen that both the dense connectivity module and the attention module are defective in F1 and accuracy metrics. In addition, for the cellular morphology that is only cultured for 24h, it is difffcult for the ffrst three methods to achieve an F1 score of 0.8 or more. Therefore, the dense attention module designed in this paper can combine the different advantages of dense connectivity and attention, which improves the accuracy and generalization of the CNN model for cell morphology recognition under various culture conditions.

D. Validation of the effectiveness of anti-hypoxic drug cultures

In order to further verify the practical value of the present method, four known antioxidant drugs were used for 48h antioxidant drug culture of AC16 hypoxic cells, and the hypoxic morphology scores were predicted by using the cell phase difference plots of the cells cultured with the antioxidant drugs by the present method, and the speciffc results are shown in Table IV, where p_1 denotes the hypoxia morphology score derived from the morphology prediction network.

From the experimental results in the table,it can be seen that the concentration of hypoxia-protective drugs increases, the predicted hypoxia phenotype score by the CNN shows a decreasing trend. This result indicates that when the concentration of hypoxia-protective drugs reaches 10μm, it exhibits a significant protective effect against hypoxia in cells, demonstrating the biological effectiveness of the method proposed in this study.

E. Validation of cellular oxidative stress indicators

In order to verify the consistency and correlation between the predictive effect of the present model and the oxidative stress indicators, H9C2 cells were cultured in hypoxia for 36h, and three cellular biochemical indicators were collected: lactate dehydrogenase (LDH), superoxide dismutase (SOD), and malondialdehyde (MDA), and hypoxia scores were predicted using the present method on the collected images.

Lactate dehydrogenase (LDH) [19]is a glycolytic enzyme primarily responsible for catalyzing the conversion of pyruvate to lactate within the body. LDH is present in the cytoplasm of all tissues and cells in the body, with relatively higher levels found in the kidneys. Superoxide dismutase (SOD) is an antioxidant enzyme present in organisms. It can convert superoxide anions into hydrogen peroxide, which is then broken down into water by catalase, thereby eliminating the harmful effects of reactive oxygen species on the human body [20]. Malondialdehyde (MDA) is one of the final products of lipid peroxidation and can serve as an indicator of oxidative stress.

Fig. 5: Correlation analysis chart of the three indicators with the predicted scores

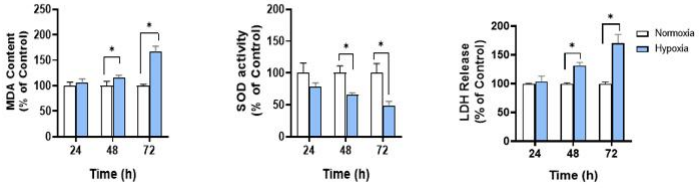

Fig. 6: Changes in biochemical indices at different incubation times

The correlation analysis of biochemical indices and hypoxia score was performed using Person correlation coefffcient and the results are shown in Figure 5. From the heat map, it can be seen that the prediction of hypoxia morphology by the DL model trained on the dataset obtained from the mixed time incubation had high correlation with LDH, SOD and MDA, with the highest correlation with SOD and MDA, negative correlation with SOD and positive correlation with MDA. From Figure 6, it can be seen that with the lengthening of incubation time, both MDA and LDH indexes are elevated due to the increase in the degree of hypoxia of cells, while SOD is negatively correlated with the incubation time, which is in line with the results of the correlation analysis mentioned above.

F. Cellular anti-hypoxia drug screening practices

Based on the deep learning multicellular portrait classiffcation model, a high-throughput compound screening system was constructed in this paper for the discrimination of antihypoxia activity of thousands of compounds. Predictive scoring was performed simultaneously by AC16 model and H9C2 model, and the two models voted on the anti-hypoxia utility of the compounds, and the compounds that received two votes were the ffnal effective anti-hypoxia compounds. Using this

TABLE IV: Results of drug validation experiments

acid type(μm)	glycyrrhizic(5)	glycyrrhizic(10)	oleanolic(5)	oleanolic(10)	acethydramine(5)	acethydramine(10)
p_1	0.893293	0.4618	0.819487	0.483541	0.686431	0.218935

TABLE V: Results of screening experiments of some anti-hypoxic compounds

Number	**Compounds**	**H9C2**	**AC16**
1-A-3	Suberosin	0.2704	0.282695
7-G-9	3,4-Dimethylbenzoic acid	0.1021	0.2535
1-C-7	3-Hydroxyhippuric acid	0.4605	0.466638
7-G-3	lsoliensinine	0.3675	0.2164

system, this paper accomplished the prediction of antioxidant activity of thousands of compounds and successfully screened out some compound molecules with antioxidant potency. The experimental data of four effective compounds,namely Suberosin,3,4-Dimethylbenzoic acid,3-Hydroxyhippuric acid and Isoliensinine are given in TableV.

Two kinds of cells were cultured in hypoxia after adding the compounds to be screened, and five pictures were collected for the culture results and two models were used for the recognition of hypoxia morphology, and the average score obtained is the data in the table. Therefore, the lower the experimental data, the lower the probability of cell hypoxia and the better the anti-hypoxia effect of the compounds.

IV. Discussion

The deep learning-based cell image screening method for hypoxia-resistant compounds is a process that utilizes machine learning techniques to identify and screen compounds that may possess antioxidant properties. This method primarily relies on the deep analysis of cell images to reveal potential patterns and features related to cell morphology and compound antioxidant activity [21].

In this study, we first preprocess the cell images, including contrast enhancement, image smoothing, edge detection, and other steps, to better highlight the structural and morphological features of the cells, thereby removing noise, improving image quality, and extracting useful features. Subsequently, we employ an optimized deep learning model, specifically a dense attention network model, to train and learn from the preprocessed images. After the model training is completed, its performance is evaluated and validated on a validation set, and the correctness of the model is verified using compounds with known utility. The model's output can serve as an indicator of the antioxidant activity of the compounds, providing a basis for subsequent screening. To ensure the accuracy of the model screening, by combining the votes and scores of multiple expert models, we can further screen out compounds that exhibit high antioxidant activity and have potential antioxidant properties in the model predictions.

In today's society, diseases related to hypoxia pose a serious threat to human health. Therefore, screening and developing drugs with hypoxia-resistant capabilities is an important task in the current pharmaceutical field. The application of the results of this project will significantly accelerate this process, improve drug development efficiency, reduce costs, and potentially provide more effective treatment options for patients.

The results of this project have broad application prospects in the field of drug screening, with far-reaching implications for the development of the pharmaceutical industry and the improvement of human health conditions. Leveraging deep learning technology, we are hopeful to make groundbreaking progress in the field of drug development, bringing good news to humanity.

Acknowledgment

The authors wish to acknowledge the support for the research work from the National Natural Science Foundation of China (CN) under grant Nos. [62076180].

References

[1] Qifeng Bai, Shuoyan Tan, Tingyang Xu, Huanxiang Liu, and Xiaojun Yao. Molaical: a soft tool for 3d drug design of protein targets by artificial intelligence and classical algorithm. *Briefings in Bioinformatics*, 2020.

[2] Zhang Shuang, Cai Lu, Pan Xue, H. E. Rui, and L. I. Chao-Ying. Effects of compound ginseng misture on anti-hypoxia and antitiredness in mice. *Ginseng Research*, 2015.

[3] Dai Kusumoto, Tomohisa Seki, Hiromune Sawada, Akira Kunitomi, and Shinsuke Yuasa. Anti-senescent drug screening by deep learning-based morphology senescence scoring. *Nature Communications*, 12(1), 2021.

[4] Thomas Blaschke, Josep Arús-Pous, Hongming Chen, Christian Margreitter, and Atanas Patronov. Reinvent 2.0: An ai tool for de novo drug design. *Journal of Chemical Information and Modeling*, 60(12), 2020.

[5] L. U. Xiu-Ying and L. I. Xiao-Ming. Research development in effects of hypoxia-inducible factors on cancer stem cells. *Medical Recapitulate*, 2008.

[6] A. Pichon, P. Connes, P. Quidu, D. Marchant, J. Brunet, B. I. Levy, J. Vilar, I. Safeukui, F. Cymbalista, and M. and Maignan. Acetazolamide and chronic hypoxia: effects on haemorheology and pulmonary haemodynamics. *European Respiratory Journal*, 40(6):1401–9, 2012.

[7] D. Penaloza and J. Arias-Stella. The heart and pulmonary circulation at high altitudes: healthy highlanders and chronic mountain sickness. *Circulation*, 115(9):1132–46, 2007.

[8] Chen Kefang, Pan Aizhen, and Hou Xiangping. Effect of total glycosides from cornus officinalis on myocardial apoptosis pathway in suckling mouse with acute hypoxia. *Pharmacology and Clinics of Chinese Materia Medica*, 2014.

[9] Zeng Wen-Jing, Liu Ju-Ying, and K. E. Chang-Bin. Establishment of myocardial hypoxia/reoxygenation injury model in rat with liquid paraffin covering method. *Journal of Yunyang Medical College*, 2010.

[10] Y. Tang, Y. Hou, Y. Zeng, Y. Hu, Y. Zhang, X. Wang, and X. Meng. Salidroside attenuates cocl2-simulated hypoxia injury in pc12cells partly by mitochondrial protection. *European journal of pharmacology*, 912:174617, 2021.

[11] Yifang Xu, Chenglei Peng, Ming Li, Yang Li, and Sidan Du. Pyramid feature attention network for monocular depth prediction. In *2021 IEEE International Conference on Multimedia and Expo (ICME)*, pages 1–6, 2021.

[12] Yan Jun, Xu Yibing, Gong Yonghong, Zhao Ningbo, Chen Shaobo, and Huang Tengjie. Method and medium for sensitivity pruning and quantization compression of neural networks, 2020.

[13] Ren Aifeng Ding Hao. Design and research of certificate text information detection system based on fpga opercl.
[14] Li Ling, Li Yanle, Guo Haili, and SU Mingmin. Identification of apple tree diseases and pests based on convolutional neural networks. *South Forum*, 53(8):4, 2022.
[15] LI Jiazhen GUO Yongxin AN Zhen, GUO Xinlei. Multi-scale convolutional neural network model for pipeline leak detection. *Journal of Hydraulic Engineering*, 54(2):220–231, 2023.
[16] Chen Bo Li Wanping. *Study of Ra dar High Range Resolution Profiles Target Recognition Based on Complex Networks*. PhD thesis, Xidian University.
[17] Wu Di, Zhao Hongtian, and Zhen Shibao. Motion deblurring method based on densenets. *Journal of Image and Graphics*, 25(5):10, 2020.
[18] Cao Shenjian. Research and implementation of target recognition based on multimodal information fusion. Master's thesis, School of Information and Software Engineering, 2023.
[19] HUANG Yan-na1, XU Guang-tao2, and YOU Chun-ping. The research progress of the lactate dehydrogenases in lactic acid bacteria. *Science and Technology of Food Industry*, 37(8):5, 2016.
[20] DONG Liang, HE Yong-zhi, WANG Yuan-liang, and DONG Zhi-yang. Research progress on application of superoxide dismutase(sod). *Journal of Agricultural Science and Technology*, (5):6, 2013.
[21] Chen Y et al Schiff L, Migliori B. Integrating deep learning and unbiased automated high-content screening to identify complex disease signatures in human fibroblasts. *Nature Communication*, (13(1)):1590, 2022.

Algorithm 1 Edge Extraction Algorithm for Multi-cell

Input:

$Input = \{x_{i,j}\}\,(i = 1, ..., W, j = 1, ..., H)$

Output:

$Edge = \{y_{i,j}\}\,(i = 1, ..., W, j = 1, ..., H)$

The Gaussian filter function $G(i,j) = \frac{1}{2\pi\sigma^2} e^{-\frac{i^2+j^2}{2\sigma^2}}$ is utilized to generate a 3×3 Gaussian filter kernel Kernel(i, j), where i and j represent the values of the horizontal and vertical coordinates, respectively, and σ represent the width of the Gaussian function.

Convolution calculation of the input image using the generated 2D Gaussian kernel: $G_{conv}(i,j) = \sum_{i=1}^{k}\sum_{j=1}^{k}(G(i,j) \times Kernel(i,j))$. Thus, the gray scale map after removing Gaussian noise $G_{conv}(i,j)$ is obtained.

The Sobel operator composed of two 3×3 matrices S_x and S_y is used to perform matrix multiplication operations in the x-direction and y-direction, respectively, on the grayscale map after Gaussian filtering processing, to obtain the gradient intensity matrix: $G_x(i,j) = S_x(i,j) \times G_{conv}(i,j)$, $G_y(i,j) = S_y(i,j) \times G_{conv}(i,j)$, $G_{xy}(i,j) = \sqrt{G_x(i,j)^2 + G_y(i,j)^2}$.

Utilizing non-maximum suppression to retain the points with the strongest pixel gradient, eliminating the spurious response from edge detection: $G_{\max}(i,j) = (G_{xy}(i,j) > G_x(i,j)\&\&G_{xy}(i,j) > G_y(i,j))?1 : 0.$

Hysteresis thresholding to eliminate pixel points whose pixel gradient strength is outside the threshold range: $G_{threshold}(i,j) = (G_{max}(i,j) > 20\&\&G_{max}(i,j) < 60)?1 : 0.$

Isolated weak edge suppression and strong edge pixel flooding:

For $y_{ij} \in G_{threshold}$

IF $y_{i+1,j-1} \in G_{max}$: $y_{i+1,j-1} = 1$

IF $y_{i+1,j-1} \in G_{max}$: $y_{i+1,j+1} = 1$

IF $y_{i-1,j+1} \in G_{max}$: $y_{i+1,j-1} = 1$

IF $y_{i-1,j-1} \in G_{max}$: $y_{i+1,j-1} = 1$

IF $y_{i-1,j} \in G_{max}$: $y_{i+1,j-1} = 1$

IF $y_{i+1,j} \in G_{max}$: $y_{i+1,j-1} = 1$

IF $y_{i,j-1} \in G_{max}$: $y_{i+1,j-1} = 1$

IF $y_{i,j-+1} \in G_{max}$: $y_{i+1,j-1} = 1$

return $Edge = \{y_{i,j}\}\,(i = 1, ..., W, j = 1, ..., H)$

Algorithm 2 Morphological feature fusion network algorithm

Input:

$Input = \{x_{i,j}\}\,(i = 1, ..., W, j = 1, ..., H)$

Output:

$p = \{p_0, p_1\}$ where p_0 denotes the probability of belonging to the normal form and p_1 denotes the probability of belonging to the hypoxic form.

1: Preliminary feature extraction:
$F_1(i,j) = \Sigma_{i=1}^{k}\Sigma_{j=1}^{k}\,(x_{i,j} \times Kernel(i,j))$

2: Advanced morphological feature extraction using the dense attention module: $F_{att} = DenseAtt(F_1)$

3: Understanding and fusion of high-level morphological features using bottleneck layers: $F_{bottle} = Bottleneck(F_{att})$

4: Further advanced morphological feature extraction using the dense attention module: $F_{att}^{'} = DenseAtt(F_{bottle})$

5: Global feature fusion:
$F_{global}(k) = \max F_{att}^{'}(k)$ where k denotes the feature map channel dimension index.

6: Hypoxia score prediction using global features of cell morphology:
$F_{final} = W \times F_{global}(k) + B$
$p_0 = \frac{e^{F_{final}(0)}}{\sum F_{final}}$, $p_1 = \frac{e^{F_{final}(1)}}{\sum F_{final}}$

7: **return** $p = \{p_0, p_1\}$ where p_0 denotes the probability of belonging to the normal form and p_1 denotes the probability of belonging to the hypoxic form.